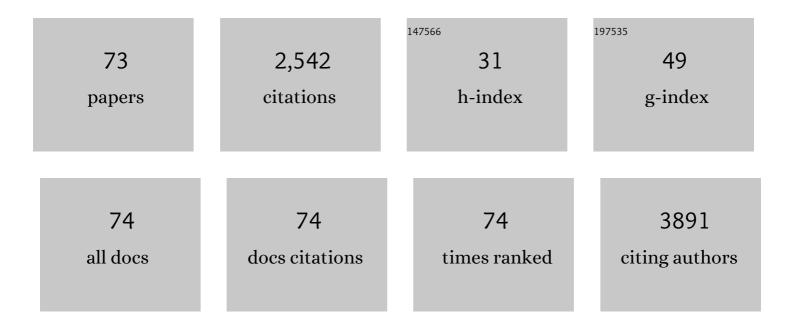
## Ahmad Esmaielzadeh Kandjani

List of Publications by Year in descending order

Source: https://exaly.com/author-pdf/5150273/publications.pdf Version: 2024-02-01



#	Article	IF	CITATIONS
1	SERS and fluorescence-based ultrasensitive detection of mercury in water. Biosensors and Bioelectronics, 2018, 100, 556-564.	5.3	155
2	Fe-doped CeO <sub>2</sub> nanorods for enhanced peroxidase-like activity and their application towards glucose detection. Journal of Materials Chemistry B, 2016, 4, 3874-3885.	2.9	151
3	Synergistic influence of polyoxometalate surface corona towards enhancing the antibacterial performance of tyrosine-capped Ag nanoparticles. Nanoscale, 2014, 6, 758-765.	2.8	146
4	Detect, Remove and Reuse: A New Paradigm in Sensing and Removal of Hg (II) from Wastewater via SERS-Active ZnO/Ag Nanoarrays. Environmental Science & Technology, 2015, 49, 1578-1584.	4.6	122
5	Oxygen-deficient photostable Cu <sub>2</sub> O for enhanced visible light photocatalytic activity. Nanoscale, 2018, 10, 6039-6050.	2.8	115
6	Zinc oxide/silver nanoarrays as reusable SERS substrates with controllable â€~hot-spots' for highly reproducible molecular sensing. Journal of Colloid and Interface Science, 2014, 436, 251-257.	5.0	97
7	Hybrid Antibacterial Fabrics with Extremely High Aspect Ratio Ag/AgTCNQ Nanowires. Advanced Functional Materials, 2014, 24, 1047-1053.	7.8	86
8	Surface modification of mixed-phase hydrogenated TiO2 and corresponding photocatalytic response. Applied Surface Science, 2015, 359, 883-896.	3.1	84
9	Sonochemical synthesis of ZnO nanoparticles: The effect of temperature and sonication power. Materials Research Bulletin, 2008, 43, 645-654.	2.7	78
10	Controlling Core/Shell Formation of Nanocubic <i>p</i> -Cu <sub>2</sub> O/ <i>n</i> -ZnO Toward Enhanced Photocatalytic Performance. Langmuir, 2015, 31, 10922-10930.	1.6	75
11	Donorâ€Induced Performance Tuning of Amorphous SrTiO <sub>3</sub> Memristive Nanodevices: Multistate Resistive Switching and Mechanical Tunability. Advanced Functional Materials, 2015, 25, 3172-3182.	7.8	68
12	Soot template TiO2 fractals as a photoactive gas sensor for acetone detection. Sensors and Actuators B: Chemical, 2018, 275, 215-222.	4.0	66
13	Effective role of trifluoroacetic acid (TFA) to enhance the photocatalytic activity of F-doped TiO2 prepared by modified sol–gel method. Applied Surface Science, 2016, 365, 57-68.	3.1	65
14	Multi-directional electrodeposited gold nanospikes for antibacterial surface applications. Nanoscale Advances, 2019, 1, 203-212.	2.2	65
15	Porous crystalline frameworks for thermocatalytic CO <sub>2</sub> reduction: an emerging paradigm. Energy and Environmental Science, 2021, 14, 320-352.	15.6	61
16	Co3O4 needles on Au honeycomb as a non-invasive electrochemical biosensor for glucose in saliva. Biosensors and Bioelectronics, 2019, 141, 111479.	5.3	54
17	Low-Temperature Fabrication of Alkali Metal–Organic Charge Transfer Complexes on Cotton Textile for Optoelectronics and Gas Sensing. Langmuir, 2015, 31, 1581-1587.	1.6	51
18	Controlled nitrogen insertion in titanium dioxide for optimal photocatalytic degradation of atrazine. RSC Advances, 2015, 5, 44041-44052.	1.7	48

#	Article	IF	CITATIONS
19	Ordered Monolayer Gold Nano-urchin Structures and Their Size Induced Control for High Gas Sensing Performance. Scientific Reports, 2016, 6, 24625.	1.6	47
20	Mercury Sorption and Desorption on Gold: A Comparative Analysis of Surface Acoustic Wave and Quartz Crystal Microbalance-Based Sensors. Langmuir, 2015, 31, 8519-8529.	1.6	43
21	Silicon as a ubiquitous contaminant in graphene derivatives with significant impact on device performance. Nature Communications, 2018, 9, 5070.	5.8	42
22	Low-Temperature Hydrogen Sensor: Enhanced Performance Enabled through Photoactive Pd-Decorated TiO <sub>2</sub> Colloidal Crystals. ACS Sensors, 2020, 5, 3902-3914.	4.0	41
23	3-D nanorod arrays of metal–organic KTCNQ semiconductor on textiles for flexible organic electronics. RSC Advances, 2013, 3, 17654.	1.7	40
24	Nanosphere Monolayer on a Transducer for Enhanced Detection of Gaseous Heavy Metal. ACS Applied Materials & Interfaces, 2015, 7, 1491-1499.	4.0	40
25	Microstructure and dynamics of vacancy-induced nanofilamentary switching network in donor doped SrTiO <sub>3â~`<i>x</i></sub> memristors. Nanotechnology, 2016, 27, 505210.	1.3	39
26	Functionalization of Elongated Tetrahexahedral Au Nanoparticles and Their Antimicrobial Activity Assay. ACS Applied Materials & Interfaces, 2019, 11, 13450-13459.	4.0	38
27	A new paradigm for signal processing of Raman spectra using a smoothing free algorithm: Coupling continuous wavelet transform with signal removal method. Journal of Raman Spectroscopy, 2013, 44, 608-621.	1.2	36
28	Ga doped RGO–TiO <sub>2</sub> composite on an ITO surface electrode for investigation of photoelectrocatalytic activity under visible light irradiation. New Journal of Chemistry, 2015, 39, 369-376.	1.4	36
29	Candle-Soot Derived Photoactive and Superamphiphobic Fractal Titania Electrode. Chemistry of Materials, 2016, 28, 7919-7927.	3.2	36
30	An investigation on linear optical properties of dilute Cr doped ZnO thin films synthesized via sol–gel process. Journal of Alloys and Compounds, 2011, 509, 7854-7860.	2.8	34
31	Transition (Mn, Fe) and rare earth (La, Pr) metal doped ceria solid solutions for high performance photocatalysis: Effect of metal doping on catalytic activity. Research on Chemical Intermediates, 2018, 44, 2523-2543.	1.3	34
32	Nano-engineered surfaces for mercury vapor sensing: Current state and future possibilities. TrAC - Trends in Analytical Chemistry, 2017, 88, 77-99.	5.8	29
33	Straddled Band Aligned CuO/BaTiO <sub>3</sub> Heterostructures: Role of Energetics at Nanointerface in Improving Photocatalytic and CO <sub>2</sub> Sensing Performance. ACS Applied Nano Materials, 2018, 1, 3375-3388.	2.4	27
34	Alkali ratio control for lead-free piezoelectric thin films utilizing elemental diffusivities in RF plasma. CrystEngComm, 2013, 15, 7222.	1.3	26
35	Electrochemical Detection of As (III) on a Manganese Oxide eria (Mn <sub>2</sub> O <sub>3</sub> /CeO <sub>2</sub> ) Nanocube Modified Au Electrode. Electroanalysis, 2018, 30, 928-936.	1.5	26
36	Zinc Titanate Nanoarrays with Superior Optoelectrochemical Properties for Chemical Sensing. ACS Applied Materials & Interfaces, 2019, 11, 29255-29267.	4.0	23

#	Article	IF	CITATIONS
37	Easy, one-step synthesis of CdTe quantum dots via microwave irradiation for fingerprinting application. Materials Research Bulletin, 2017, 90, 260-265.	2.7	21
38	A Nanoengineered Conductometric Device for Accurate Analysis of Elemental Mercury Vapor. Environmental Science & Technology, 2016, 50, 1384-1392.	4.6	20
39	Silver/gold core/shell nanowire monolayer on a QCM microsensor for enhanced mercury detection. RSC Advances, 2015, 5, 92303-92311.	1.7	18
40	Development and comparative investigation of Ag-sensitive layer based SAW and QCM sensors for mercury sensing applications. Analyst, The, 2016, 141, 2463-2473.	1.7	18
41	1,4-Dihydropyrrolo[3,2- <i>b</i> ]pyrroles as a Single Component Photoactive Layer: A New Paradigm for Broadband Detection. ACS Applied Materials & Interfaces, 2017, 9, 27875-27882.	4.0	18
42	Powder production via electrohydrodynamic-assisted molten metal jet impingement into a viscous medium. Powder Technology, 2010, 203, 518-528.	2.1	15
43	Hydrogen Bubble Templated Growth of Honeycomb-Like Au-Pt Alloy Films for Non-Enzymatic Glucose Sensing. Journal of the Electrochemical Society, 2016, 163, B689-B695.	1.3	15
44	Au Nanospikes as a Nonâ€enzymatic Glucose Sensor: Exploring Morphological Changes with the Elaborated Chronoamperometric Method. Electroanalysis, 2017, 29, 294-304.	1.5	13
45	Solution-processable do-it-yourself switching devices (DIY devices) based on CuTCNQ metal-organic semiconductors. Applied Materials Today, 2018, 10, 12-17.	2.3	13
46	Cold vapor integrated quartz crystal microbalance (CV-QCM) based detection of mercury ions with gold nanostructures. Sensors and Actuators B: Chemical, 2019, 290, 453-458.	4.0	13
47	Studying the effect of dealloying Cu-Au nanostructures on their mercury sensing performance. Sensors and Actuators B: Chemical, 2017, 245, 273-281.	4.0	12
48	Gold Sunflower Microelectrode Arrays with Dendritic Nanostructures on the Lateral Surfaces for Antireflection and Surface-Enhanced Raman Scattering. ACS Applied Nano Materials, 2022, 5, 1873-1890.	2.4	12
49	Galvanic replacement of colloidal monolayer crystal on a QCM device for selective detection of mercury vapor. Sensors and Actuators B: Chemical, 2017, 250, 383-392.	4.0	11
50	Functionalized Concave Cube Gold Nanoparticles as Potent Antimicrobial Agents against Pathogenic Bacteria. ACS Applied Bio Materials, 2022, 5, 492-503.	2.3	11
51	Photocatalytic decoloration of Acid Red 27 in presence of SnO2 nanoparticles. Water Science and Technology, 2010, 62, 1256-1264.	1.2	9
52	A nanoengineered surface acoustic wave device for analysis of mercury in gas phase. Sensors and Actuators B: Chemical, 2016, 234, 562-572.	4.0	9
53	The Preparation of a AuCN/Prussian Blue Nanocube Composite through Galvanic Replacement Enhances Stability for Electrocatalysis ChemistrySelect, 2017, 2, 5333-5340.	0.7	9
54	Preparation of Au nanoparticles on a magnetically responsive support via pyrolysis of a Prussian blue composite. Journal of Colloid and Interface Science, 2019, 540, 563-571.	5.0	9

#	Article	IF	CITATIONS
55	Nickel–gold bimetallic monolayer colloidal crystals fabricated via galvanic replacement as a highly sensitive electrochemical sensor. Journal of Materials Chemistry B, 2017, 5, 5441-5449.	2.9	8
56	Longâ€Range Ordered Crystals of 3D Inorganic–Organic Heterojunctions via Colloidal Lithography. Small Methods, 2019, 3, 1900080.	4.6	8
57	Long-range ordered TiO <sub>2</sub> /Au hollow urchins: topology control for maskless electrodeposition. Journal of Materials Chemistry A, 2020, 8, 26035-26044.	5.2	8
58	Liquid Crystal-Mediated 3D Printing Process to Fabricate Nano-Ordered Layered Structures. ACS Applied Materials & Interfaces, 2021, 13, 28627-28638.	4.0	7
59	Fluorescence brightness and photostability of individual copper (I) oxide nanocubes. Scientific Reports, 2017, 7, 16905.	1.6	6
60	Recyclable SERS substrate: Optimised by reducing masking effect through colloidal lithography. Applied Surface Science, 2022, 578, 151852.	3.1	6
61	Gas sensing performance enhancement: Determining the role of active sites through colloidal lithography. Sensors and Actuators B: Chemical, 2018, 273, 1376-1384.	4.0	5
62	Synthesis and Characterization of TiO <sub>2</sub> Nanoparticles via Chemical Bath Deposition (CBD) Method. Journal of Nano Research, 2010, 11, 35-38.	0.8	4
63	Preferential synthesis of highly conducting Tl(TCNQ) phase II nanorod networks via electrochemically driven TCNQ/Tl(TCNQ) solid-solid phase transformation. Journal of Solid State Electrochemistry, 2016, 20, 3303-3314.	1.2	4
64	Nanostructured Fused Pyrrole Thin Films: Encoding Nano "Bits―with Temporary Remanence. Advanced Electronic Materials, 2018, 4, 1700626.	2.6	4
65	Characteristics of the breakup and fragmentation of an electrohydrodynamic melt jet. Particuology, 2012, 10, 255-265.	2.0	3
66	Fabrication of fractal structured soot templated titania-silver nano-surfaces for photocatalysis and SERS sensing. Applied Surface Science, 2022, 594, 153383.	3.1	3
67	Organic ligand interaction with copper(II) ions in both aqueous and non-aqueous media: Overcoming solubility issues for sensing. Sensors and Actuators B: Chemical, 2022, 365, 131934.	4.0	2
68	Linear optical properties of ZnO nano particles synthesized by electrohydrodynamics atomization (EHDA) method. Journal of Materials Science: Materials in Electronics, 2012, 23, 384-389.	1.1	1
69	Volatile Memory: Nanostructured Fused Pyrrole Thin Films: Encoding Nano "Bits―with Temporary Remanence (Adv. Electron. Mater. 8/2018). Advanced Electronic Materials, 2018, 4, 1870038.	2.6	1
70	Using colloidal lithography to control the formation of gas sorption sites through galvanic replacement reaction. Journal of Colloid and Interface Science, 2019, 547, 199-205.	5.0	1
71	Gold nanorod self-assembly on a quartz crystal microbalance: an enhanced mercury vapor sensor. Environmental Science: Nano, 0, , .	2.2	1
72	A real-time comparison of mercury accumulation on noble metal thin films using gravimetric device. Superlattices and Microstructures, 2016, 100, 1151-1158.	1.4	0

#	Article	IF	CITATIONS
73	Inorganic/Organic Heterojunctions: Longâ€Range Ordered Crystals of 3D Inorganic–Organic Heterojunctions via Colloidal Lithography (Small Methods 10/2019). Small Methods, 2019, 3, 1970034.	4.6	0